

An Atlas of Spectrophotometric Landolt Standard Stars

Maximilian Stritzinger,^{1,2} Nicholas B. Suntzeff,³ Mario Hamuy,⁴ Peter Challis,⁵ Ricardo Demarco,⁶ Lisa Germany,⁷ A. M. Soderberg,⁸

¹*Max-Planck-Institut für Astrophysik, Karl-Schwarzschild-Str. 1, 85741 Garching, Germany*

²*Visiting Astronomer, Cerro Tololo Inter-American Observatory*

³*Cerro Tololo Inter-American Observatory⁹, Casilla 603, La Serena, Chile*

⁴*Las Campanas Observatory, Carnegie Observatories, Casilla 601, La Serena, Chile*

⁵*Harvard-Smithsonian Center for Astrophysics, 60 Garden Street, Cambridge, MA 02138, USA*

⁶*Department of Physics and Astronomy, Johns Hopkins University, 3400 N. Charles St., Baltimore, MD 21218, USA*

⁷*European Southern Observatory, Alonso de Cordova 3107, Vitacura Santiago, Chile*

⁸*Caltech Institute of Technology, 1201 E. California Blvd, Pasadena, CA 91125, USA*

stritzin@mpa-garching.mpg.de
 nsuntzeff@noao.edu
 mhamuy@lco.cl
 pchallis@cfa.harvard.edu
 demarco@pha.jhu.edu
 lgermany@eso.org
 ams@astro.caltech.edu

ABSTRACT

We present CCD observations of 102 Landolt standard stars obtained with the R-C spectrograph on the CTIO 1.5 m telescope. Using stellar atmosphere models we have extended the flux points to our six spectrophotometric secondary standards, in both the blue and the red, allowing us to produce flux-calibrated spectra that span a wavelength range from 3050 Å to 1.1 μ m. We find mean differences between *UBVRI* spectrophotometry computed using Bessell's standard passbands and Landolt's published photometry to be 1% or less. Observers in both hemispheres will find these spectra useful for flux-calibrating spectra

⁹Cerro Tololo Inter-American Observatory, Kitt Peak National Observatory, National Optical Astronomy Observatories, operated by the Association of Universities for Research in Astronomy, Inc., (AURA), under cooperative agreement with the National Science Foundation.

and through the use of accurately constructed instrumental passbands be able to compute accurate corrections to bring instrumental magnitudes to any desired standard photometric system (S-corrections). In addition, by combining empirical and modeled spectra of the Sun, Sirius and Vega, we calculate and compare synthetic photometry to observed photometry taken from the literature for these three stars.

Subject headings: standard stars: spectrophotometry –techniques: photometric

1. Introduction

From dedicated follow-up observations of supernovae (hereafter SNe) it has become clear that systematic magnitude differences can exist between data sets obtained at different telescopes for the same event. These differences can be on the order of several hundredths of a magnitude or more near maximum light and potentially larger for late-time photometry when the spectrum enters the nebular phase. This effect is undoubtedly caused by the use of filter sets employed at different telescopes, which do not exactly match each other (Suntzeff et al. 1988; Menzies 1989; Hamuy et al. 1990; Suntzeff 2000), and are magnified when the instrumental filters differ grossly from the standard Johnson/Kron-Cousins passbands. Although the observed photometry is standardized to a common system through the use of color terms, this is not expected to work perfectly. This is because there are radical differences between the normal and continuous spectral energy distributions (SEDs) of the photometric standard stars compared to the SEDs of SNe, which are dominated by strong absorption and emission features.

Using SNe photometry uncorrected for this effect can lead to incorrect calculations of colors, host galaxy reddening, absolute magnitudes, and can ultimately bias cosmological parameters. However, the photometrist may remedy this by computing “S-corrections” to correct their photometry to a standard filter transmissivity function. An at least partially successful attempt to reconcile these magnitude differences in the optical for the well observed SN 1999ee was made by Stritzinger et al. (2002). More recently, this photometric technique has been used in the optical and extended to near infrared photometry by Krisciunas et al. (2003), Candia et al. (2003), Krisciunas et al. (2004), and Pignata et al. (2004) for a number of other well observed SNe.

Spectrophotometric standard stars play a crucial role in determining accurate S-corrections. However, there exists only a small number of moderately faint standard stars –which are of limited color range– useful for spectroscopic calibrations. In this work we construct a large

atlas of flux-calibrated spectra in order to enlarge the hitherto available spectrophotometric standards. Our program consists of a large number (~ 100) of Landolt standard stars, which have well-documented photometric magnitudes and are widely used for photometric calibrations. These standard stars now may be employed to flux-calibrate spectra necessary for determining many physical parameters of stars, (e.g. surface temperatures, radial velocities, abundances, surface gravities, etc.) relate spectral and photometric observations, and to calculate $UBVRIz$ -band S-corrections for any celestial object whose SED significantly differs from the standards used to calibrate the observed photometry. These spectra are now available for other researchers, provided in electronic form as FITS files.¹⁰

The motivation of the authors for this study was to be able to model a typical night's run of photometry at a facility telescope and CCD instrument. We would like to be able to start with the SEDs of the program objects, usually SNe, and the Landolt stars. Then, with system transmission functions, which include atmospheric extinction, mirror reflectivities, filter functions, dewar windows, and the detector quantum efficiencies, calculate synthetic magnitudes as close as possible to the observed natural system. Finally, we want to use the synthetic natural system magnitudes and run them through our photometric codes to calculate the typical extinction and color terms that we solve for each night. By comparing the synthetic to the observed transformations, we can assess the effects of many possible systematic errors in our data. How close do the color terms match? How does the changing extinction across the photometric bands affect the calculated colors at higher airmass? It should also be possible, in principle, to calculate the transmission functions of the photometric bands from scratch using the observed photometric solutions and the SEDs (Jha 2002).

As an example, which may surprise most astronomers who do not do photometry, very few photometrists use second-order (color dependent) terms in the extinction because it is difficult to measure this effect accurately. Most extinction is handled as a simple grey shift of the form $m(nat)_0 = m(nat) - k * X$, where X is the extinction and k is the extinction coefficient of a given bandpass. We include the extinction curve in our system throughput curves when doing synthetic photometry, but we do not gauge its effects on the color for stars observed at $X = 1$ versus $X = 2$. With this atlas of Landolt SED spectra we will now be able to calculate the second order terms using synthetic photometry.

The structure of this paper is as follows. In § 2 we present our observations, followed by the spectroscopic reductions in § 3. Our results for the program stars are given in § 4. Finally, in § 4 we also compute synthetic photometry of the Sun, Sirius and Vega and compare these

¹⁰At <http://www.mpa-garching.mpg.de/~stritzin/data/>

values to magnitudes found in the literature.

2. Observations

We have adopted six bright ($4.3 \lesssim V \lesssim 5.7$) secondary standard stars (see Table 1) originally published in Hayes (1970), and later re-calibrated by Taylor (1984); Hamuy et al. (1992, 1994) as our defining spectrophotometric system. Note that these stars are secondary standards because they tie the Kitt Peak National Observatory and CTIO spectrophotometric standards (Massey et al. 1988; Hamuy et al. 1992, 1994) to Vega. The program consists of 102 Landolt standard stars located along the celestial equator ranging $7.0 \lesssim V \lesssim 13.0$. We refer the reader to Landolt (1983, 1992a,b), Hamuy et al. (1992), and references within for spectral classifications, $UBVRI$ -band photometry, coordinates, and finding charts. The reference and observed photometry for each star may also be found in the image header of each spectrum.

All observations were obtained with the CTIO 1.5 m, using the R-C spectrograph, during 5-13 February 1999 (UT). Of the eight nights observed, all were photometric except the last night of 12-13 February 1999 (UT). Half of the observations were dedicated to a blue setup while the other half were allocated to a red setup. The blue setup employed a low dispersion grating (300 lines mm^{-1}) with a dispersion of 2.85 Å per pixel blazed at 4000 Å and a 1200×800 LORAL CCD. We observed in first order with a total wavelength coverage of 3300 Å (3100-6400 Å) and a FWHM resolution of 8.6 Å. The red setup consisted of a low dispersion grating (158 lines mm^{-1}) with a dispersion of 5.34 Å per pixel blazed at 8000 Å with the same LORAL CCD. We observed in first order with a total wavelength coverage of 4800 Å (5800-10,600 Å) and a FWHM resolution of 16.4 Å. Note that it was necessary to use an OG570 second order blocking filter to suppress any leakage, which would have otherwise contaminated the spectra red-ward of 6000 Å.

Daily observations began with obtaining calibration images. This included bias frames, dome flats with a 2" and 21" slit and finally twilight flats through a 21" slit. Nights in which we observed with the blue set up we took projector flats with a quartz lamp. Note that with the projector flats we used CuS_0_4 and Corning 9863 filters to prevent saturation of the CCD. The observing procedure consisted of (1) pointing the telescope to the coordinates of the standard star, (2) close the slit to 2" and then take an exposure with a HeAr lamp, (3) select a random field star for telescope guiding purposes, and (4) take an exposure of the standard star with a slit width of 21". On the first two nights the secondary standards were each observed at three slit positions and the program stars at two slit positions. By the

third night *all* stars were observed with four slit positions.¹²

Each night we typically observed five or six secondary standard stars (see Table 1), obtaining between 50 and 70 spectra at a wide range of airmass between $z = 1.0$ and $z = 2.3$, in order to solve for the nightly extinction curve. When observing the program stars we restricted the range of airmass to between $z = 1.0$ and $z = 1.3$ in order to reduce the differential effects of the Earth’s atmosphere such as telluric absorption and atmospheric refraction between the program and spectrophotometric standard stars. Integration times were chosen such that for the majority of 1-D spectra (resulting from adding all the flux in the 2-D image along the spatial direction) the number of counts was between 40,000 and 50,000 ADU per resolution element. Thus, the exposure times for the bright secondary standards ranged between 2 and 7 seconds, while exposure times for the program stars typically ranged between 25 and 400 seconds. Due to the short integration times of the secondary standards it proved necessary to apply a shutter correction to their spectra (see below §3). From multiple exposures taken with 1-s, 2-s, 3-s, 4-s and 6-s exposure times on 6-7 February 1999 (UT) an additive mean shutter error for a one second exposure was determined to be -0.023 seconds ± 0.010 (s.d.).

3. Spectroscopic Reductions

Standard spectroscopic reduction techniques using IRAF¹³ were performed to reduce the data. To begin we subtracted the over-scan and bias from all spectra including the HeAr frames. With the blue setup we constructed a flat field image using a combination of dome flats (external illumination), projector flats (internal illumination), and sky flats. The projector flats provide illumination in the ultraviolet end of the CCD ($\lambda < 3800 \text{ \AA}$), the dome flats at redder wavelengths, and the sky flat permitted us to correct the dome and projector flats for uneven illumination along the slit. With the red setup we only used dome and sky flats. The resulting flats (normalized along the dispersion axis) were divided into all of the observed spectra. Next we extracted 1-D spectra from the 2-D flat fielded images

¹²A preliminary data reduction showed that all of the spectra from 5800 to 7000 \AA were choppy at the 2-4% level. Note that this choppiness was similar to broad-scale fringing which is typically seen at wavelengths longward of 8000 \AA . To alleviate this problem, the observing procedure was changed to observe all stars at four slit positions at lower flux levels in order to obtain similar total integration times. The co-added frames reduced the level of choppiness by half.

¹³The Image Reduction and Analysis Facility (IRAF) is distributed by the National Optical Astronomy Observatory, which is operated by AURA Inc., under a cooperative agreement with the National Science Foundation.

and dispersion-calibrated them to a linear wavelength scale using the HeAr calibrations frames that were taken before each exposure. Shutter corrections were then applied to all the secondary standards by multiplying a factor of

$$\frac{ET}{ET + ST} \quad (1)$$

into each spectra, where ET is the requested exposure time in seconds and ST is the mean shutter error given in § 2.

If the program stars are to be used as spectrophotometric standards for calculating U - and z -band spectrophotometry it proved necessary to extend the wavelength range of their spectra beyond the 3300-10,406 Å range of the secondary standards. This was accomplished by fitting synthetic spectra modeled with appropriate physical parameters, to each of our secondary standards, using Robert Kurucz's stellar atmosphere code BILL.f. By extrapolating from the models we obtained six new flux points. These included four flux points blue-ward of 3300 Å at 3250, 3200, 3150 and 3100 Å and two flux points red-ward of 10,406 Å at 10,500 and 10,600 Å. Note that it was necessary to scale the models to the observed blue and red tilt spectra by multiplication of an arbitrary constant. This constant was derived such that the modeled spectrum could reproduce the same values (up to two significant figures) as the flux points given in Table 5 of Hamuy et al. (1992). In addition, because two of the Hamuy et al. (1994) flux points were placed in regions of strong atmospheric absorption, we relocated them from 7782 and 9834 Å to 7845 and 9915 Å, respectively. We also added two additional flux points at 9970 and 10,150 Å. Because there are no flux points from 8376-9834 Å we attempted to add two flux points in this interval at locations free of atmospheric and stellar absorption features, at 8800 and 8920 Å, each with a 10 Å bandwidth. Unfortunately, when deriving the nightly response curve these flux points showed systematic residuals up to $\sim 0^m 10$ compared to neighboring flux points and were thus omitted.

In Table 1 we present re-calibrated monochromatic magnitudes of our spectrophotometric secondary standards from 3100 to 10,600 Å. These values are defined by

$$m_\nu = -2.5\log_{10}[f_\nu] - ZP, \quad (2)$$

where f_ν is the monochromatic flux in $\text{ergs cm}^{-2} \text{ s}^{-1} \text{ Hz}^{-1}$, and ZP is the zero-point for the magnitude scale. We have chosen the zero-point for the monochromatic magnitude scale to be -48.590 (Massey et al. 1988).

Before we flux calibrate the spectra, it is important to remove as much of the instrumental artifacts (such as fringing) and telluric absorption as possible. The most difficult signature to remove is the flat-fielding error, which introduces very high-order variations in the continuum at the few percent level, due to the continuum fitting algorithms used to take

a flat field lamp and “flatten” it with an IRAF task like RESPONSE. Typically we used a polynomial of order 20 to 30 to fit out the flat field response. This will introduce wiggles with a period of roughly 150 Å or so, which are impossible to remove with a polynomial fit to the Hayes flux points, which are often more than 200 Å separated. In the region of 8000-9500 Å the flux points are even more separated, and one cannot fit out these flat-fielding errors.

However, Bessell (1999) who noticed correlated errors in the Hamuy et al. spectrophotometric standards, has suggested an ingenious way of removing these flat-fielding errors. He proposed that the data be divided by a spectral flat, preferably with a spectrum of an astrophysical source that is close to a black body or otherwise line free. There is no such source, but there are some stars listed in his table such as Feige 110 or VMa2, which are close to being a pure continuum source. Most of these stars were too faint for the 1.5 m so we had to do the next best thing – use the division of an observed spectrum of a hot star with the model of the hot star. We used HR 3454, which was observed every night at an airmass ~ 1.2 . To construct the red spectral flat we first made a theoretical spectrum using the Kurucz code at the same dispersion and wavelength coverage as the observed spectra. Because the Kurucz models are only available for a large grid of physical parameters, it was necessary to interpolate from the models to produce a spectrum that most accurately matched HR 3454.¹⁴ All the red dispersion-calibrated spectra of HR 3454 at an airmass of 1.2 were then averaged and divided by the modeled spectrum. A few of the strongest spectral features, such as H α , did not cleanly disappear in the spectral flat. Therefore we removed these residuals by interpolation. Next, all of the red dispersion-calibrated data for each night were divided by this spectral flat field. Fig. 1 displays the main telluric features red-ward of 6000 Å that were removed from all the red spectra by division of the spectral flat. The most prominent telluric features were those associated with atmospheric H₂O and O₂. We found the O₂ A- and B-bands to be saturated for all observations, whereas the strength of the H₂O features were strongly dependent on both the airmass and the time at which the star was observed.

The blue spectral flat was constructed by averaging all the dispersion-calibrated observations of HR 3454 made at an airmass of 1.2. This was then divided into all of the blue tilt dispersion-calibrated data. Through the use of spectral flat fields we obtained smooth dispersion-calibrated spectra free of large telluric absorption and instrumental features.

We proceeded to flux-calibrate the data using the newly calibrated spectrophotometric secondary standards. Data from each night was first corrected for atmospheric extinction,

¹⁴This spectrum corresponds to a model produced for physical parameters (T_{eff} , $\log g$, [M/H]) = (18650 K, 3.5, 0).

via the nightly extinction curves derived from the secondary spectrophotometric standards, which were observed to this end over a range of airmasses. In Fig. 2 we present an averaged extinction curve obtained from the seven photometric nights for both the blue and the red setups, and in Table 2 we list this extinction curve in tabular form. To obtain flux-calibrated spectra, we derived a nightly response curve by fitting a low order cubic spline to the observed flux values obtained from the secondary standards. When deriving nightly response curves we were able to extend the wavelength range past our reddest flux point given in Table 1 by 400 Å to 11,000 Å and by 50 Å in the blue to 3050 Å. To calculate spectrophotometry for each star it was necessary to stitch the blue and red spectra together. This was accomplished by first comparing all the blue and red spectra for an individual star at an airmass of 1.5 or less. If there were any spectra that did not agree with the others they were omitted. We then combined all the spectra by averaging them together (using the IRAF task `scombine`) to produce a master spectrum for each star. Each master spectrum covers a total wavelength range of 7950 Å (3050-11,000 Å). Note that when considering all of individual spectra together the flux offsets were typically extremely small, on the order of ~ 0.001 mag.

An indication that the Bessell method of using spectral flats works well is that the flux calibrations curves were fit with low order polynomials. Without the division of the spectral flats, there were noticeable wiggles in the sensitivity curve that required high order (12 or so) polynomials. With the division of the spectral flats, we could use much lower polynomial fits. This gives us confidence that the fits into the red regions where there are fewer flux points will introduce smaller systematic effects in the flux scale.

4. Results

4.1. Program Stars

In this section we want to assess the spectrophotometric properties of our spectra by comparing broad-band synthetic magnitudes to those measured by Landolt. As all objects were measured with a photon detector, a synthetic magnitude on the natural system must be calculated as the convolution of a star’s photon flux (N_λ) with the filter instrumental passband ($S(\lambda)$), i.e.

$$\text{mag} = -2.5 \log_{10} \int N_\lambda S(\lambda) d\lambda + ZP, \quad (3)$$

where ZP is the zero-point for the magnitude scale. As a minimum, $S(\lambda)$ should include the transparency of the Earth’s atmosphere, the filter transmission, the quantum efficiency

(QE) of the detector, and mirror reflectivities.

Note that there is often confusion about the form of $S(\lambda)$. Some references use a function of the form $R(\lambda) = \lambda^* S(\lambda)$ and integrate $R(\lambda)^* F(\lambda)$, where $F(\lambda)$ is in units of $\text{ergs s}^{-1} \text{cm}^{-2} \text{\AA}^{-1}$. In equation 3 we are specifying the photon flux in units of $\text{photons s}^{-1} \text{cm}^{-2} \text{\AA}^{-1}$. With this definition, the meaning of $S(\lambda)$ is very easy to understand – it is just the fraction of photons (or energy) that is detected with respect to the incident flux outside the earth’s atmosphere. $S(\lambda)$ accounts for all the flux lost due to the flux passing through the atmosphere, telescope, and instrument.

To construct the standard passbands we adopted the Johnson/Kron-Cousins *UBVRI* transmission functions given in Bessell (1990) (see our Fig. 3). Note, however, that the Bessell transmission functions are intended for use with energy rather than photon distributions (see Appendix in Bessell 1983). Thus, it was necessary to divide these functions by λ before employing them in Eq. (3) (Suntzeff et al. 1999; Hamuy et al. 2001). Because telluric absorption features were removed from the spectra, an atmospheric opacity spectrum was included in the construction of the standard passbands.

Armed with the standard passbands we proceeded to calculate synthetic magnitudes for our spectra using zero-points determined from secondary spectrophotometric standards (Landolt 1992b; Hamuy et al. 1994; Landolt 1999) rather than Vega, which has uncertain *UBVRI*-band optical photometry. When calculating zero-points we did not include telluric absorption in the passbands because Hamuy et al. did not remove these features from their spectra. Table 3 lists the resulting zero-points. In Table 4 we list synthetic magnitudes for all standard stars computed with Eq. (3) and the standard passbands, as well as the difference between observed and synthetic magnitudes. Note that the optical photometry for the secondary standards was taken from Hamuy et al. (1992). Sufficient wavelength coverage was obtained for 98 of the 108 standard stars listed in Table 4 to calculate *UBVRI* magnitudes. The remaining ten stars were observed in either the blue or red tilt except HD57884 and HD60826 whose spectra were cut off blue-ward of 4000 Å. In Table 4 we also identify stars that are known or thought to be variable stars.

In Fig. 4 we present, for all standards observed, the difference between observed and synthetic magnitudes computed with the standard passbands, as a function of observed color. Overall there is a high internal accuracy between the observed and synthetic magnitudes as seen in Table 5, which lists the mean difference and associated standard deviation for each band. We find that the mean difference between the observed photometry and our *UBVRI*-band synthetic magnitudes is 1% or less. However, it is evident from Fig. 4 that slight color terms do exist, most notably in the *U*- *B*- and *R*-bands. This color dependence reflects a small mismatch between the Bessell functions and the standards Johnson/Kron-Cousins system

and/or a possible error in the fundamental spectrophotometric calibration. To remedy this problem our approach consisted of applying wavelength shifts to the Bessell functions until we obtained a zero color dependence. Table 6 lists the resulting shifts. Although small compared to the Bessell bandwidths ($\sim 1000 \text{ \AA}$), they have a non-negligible effect on the synthetic magnitudes, and the shifted standard passbands can be considered the best models for the Johnson/Kron-Cousins system. In Table 7 we provide our new modeled UBV standard passbands. In Table 8 we list the R and I standard passbands. Note, that the R and I standard passbands include an atmospheric line opacity spectrum. In Fig. 5 we present the comparison of Bessell’s standard passbands (dotted lines) to our new modeled passbands (dashed lines). In addition, to complement the shifted passbands we provide a convenient list of wavelength shifts (see Table 9) one would apply to the standard passbands in order to increase the color term by 0.01 mag mag^{-1} . Note in Table 9 the color term (for example the B -band) is in the form of $B = zpt + b_{nat} + K(B - V)$. Also listed is the color used in each color term.

With the V -band spectrophotometry and dispersion-calibrated spectra we investigated the LORAL CCD’s response for all the nights on which observations were conducted. In Fig. 6 we present the difference between standard and synthetic V -band magnitudes as a function of counts in the extracted 1-D spectra at the effective V -band wavelength for all observations. We conclude from Fig. 6 that the response function of the LORAL CCD was linear to within 2%.

4.2. The Sun, Sirius and Vega

In addition to the selected Landolt standard stars in this work, we have calculated spectrophotometry for the Sun, Sirius and Vega. As there are no spectrophotometric standards in the infrared comparable to that in the optical, these objects can be useful to accurately characterize the modeled passbands when computing JHK -band S-corrections (see Krisciunas et al. (2004)). Spectra for these objects have been constructed using a combination of empirical and modeled data. The reader is referred to Appendix A in Krisciunas et al. (2003) for a more detailed description of the construction of these spectra; below we provide a brief summary for each of these stars.

Our solar spectrum combines empirical data from Livingston & Wallace (1991) scaled to a solar model from the Kurucz Web site (Kurucz et al. 1984) with physical parameters (T_{eff} , $\log g$, v_{micro} , mixing length/scale height) = 5777 K, 4.438, 1.5 km s^{-1} , 1.25. For Vega we have adopted observational data from Hayes (1985). His data were combined with the Kurucz spectrum vega090250000p.asc5 with physical parameters (T_{eff} , $\log g$, v_{micro} , mixing

length/scale height) = 9550 K, 3.950, -0.5, 2 km s⁻¹, 0. The Kurucz model was then scaled to match the flux points of Hayes (1985). The Sirius spectrum was constructed using the Kurucz model sir.ascsq5 scaled to force the synthetic V magnitude to equal the observed value of -1.430 (Bessell et al. 1998). Note that each of these spectra were convolved to 2 Å and re-sampled to 1 Å per pixel.

To compute *UBVRI* synthetic photometry we employed our new modeled passbands (shown in Fig. 5) and the zero-points listed in Table 3. To calculate *JHK*-band synthetic magnitudes we constructed instrumental passbands, (see Fig. 7), which included information associated with the Las Campanas Observatory’s 1 m Henrietta Swope telescope where the Persson et al. (1998) infrared system was established. This includes Persson et al. J_S , H , and K_S filter transmissivities, a Rockwell NICMOS2 QE response function, two aluminum reflections, a Dewar window transmissivity, multiple reflections associated with optical elements within the C40IRC camera, and an atmospheric line opacity spectrum. Zero-points were calculated by forcing the synthetic magnitudes of Vega to equal that of the Elias et al. (1982) CIT photometric system, i.e. $(J, H, K) = (0, 0, 0)$. The resulting *JHK*-band zero-points were -11.954, -11.895, and -12.063, respectively.

Table 10 lists the published photometry (from multiple sources), our synthetic photometry and the difference between the two in the sense of observed minus synthetic. The difference between Vega’s *V*-band observed and synthetic magnitudes shows that our zero-points, calculated using the secondary standards from Hamuy et al. (1994), have an associated error ~ 0.01 mag. The large differences in the *UB*-bands may be due to the difficulty in obtaining accurate measurements of a star as bright as Vega. We find poor agreement for the Sun between *UJHK* observed and synthetic magnitudes. This as well is not surprising considering the difficulty in obtaining precise photometry of a source as bright and extended as the Sun. Some of the large *U*-band difference may be a result of the large variability of both the Sun’s flux in the ultraviolet and Earth’s atmospheric transmissivity. The differences in the infrared may be attributed to telluric absorption features that were not sufficiently accounted for in our manufactured instrumental passbands. The near infrared spectrophotometry of Sirius matches well with observed photometry to within 1% or less, while in the optical the difference is on the order of 4% or less.

A special thanks goes to Arlo Landolt for providing us updated values for the spectrophotometric standards. We also acknowledge Mike Bessell, Kevin Krisciunas, Brian Schmidt, Eric Persson, and Fiorella Castelli for helpful discussions on photometry and spectrophotometry. We thank Bruno Leibundgut for helpful comments on a preliminary draft of this manuscript. M.S. acknowledges financial support from HST grant GO-07505.02-96A, and the International Max-Planck Research School on Astrophysics. This research has made use

of the SIMBAD database, operated at CDS, Strasbourg, France.

REFERENCES

Bessell, M. S. 1983, PASP, 95, 480

Bessell, M. S. 1990, PASP, 102, 1181

Bessell, M. S., Castelli, F. & Plez, B. 1998, A&A, 337, 321 (erratum)

Bessell, M. S. 1999, PASP, 111, 1426

Candia, P., et al. 2003, PASP, 115, 277

Cohen, M., Walker, R. G., Carter, B., et al. 1999, AJ, 117, 1864

Colina, L., Bohlin, R. C. & Castelli, F. 1996, AJ, 112, 307

Cayrel de Strobel, G. 1996, A&A Rev., 7, 243

Elias, J. H., Frogel, J. A., Matthews, K. & Neugerbauer, G. 1982, AJ, 87, 1029

Hamuy, M., Suntzeff, N. B., Bravo, J. & Phillips, M. M. 1990, PASP, 102, 888

Hamuy, M., et al. 1992, PASP, 104, 533

Hamuy, M., et al. 1994, PASP, 106, 566

Hamuy, M., et al. 2001, ApJ, 558, 615

Hayes, D. S. 1970, ApJ, 159, 165

Hayes, D. S. 1985, IAU Symp. 111: Calibration of Fundamental Stellar Quantities, 111, 225

Jha, S. 2002, PhD. Thesis, Harvard University

Kurucz, R. L., et al. 1984, Solar Flux Atlas from 296 to 1300 nm (Sunspot, NM:Natl. Solar Obs.)

Krisciunas, K., Suntzeff, N. B., et al. 2003, AJ, 125, 166

Krisciunas, K., et al. 2004, AJ, 127, 1664

Landolt, A. U. 1983, AJ, 88, 439

Landolt, A. U. 1992, AJ, 104, 340

Landolt, A. U. 1992, AJ, 104, 372

Landolt, A. U. 1999, (private communication)

Livingston, W. & Wallace, L. 1991, NSO Technical Report, Tucson: National Solar Observatory, National Optical Astronomy Observatory

Massey, P., et al. 1988, ApJ, 328, 344

Menzies, J. W. 1989, MNRAS, 237, 21

Persson, S. E., Murphy, D. C., Krzeminski, W., Roth, M. & Rieke, M. J. 1998, AJ, 116, 2475

Pignata, G., et al. 2004, MNRAS, 355, 178

Stebbins, J., Kron, G.E. 1957, ApJ, 126, 226

Stritzinger, M., Hamuy, M., Suntzeff, N. B., et al. 2002, AJ, 124, 2100

Suntzeff, N. B., Hamuy, M., Martin, G., Gómez, A. & González, R. 1988, AJ, 96, 1864

Suntzeff, N. B., et al. 1999, AJ, 117, 1175

Suntzeff, N. B. 2000, in *Cosmic Explosions*, Tenth Astrophysics Conference, ed. S.S. Holt & W.W. Zhang (AIP, New York), 65

Taylor, B. J. 1984, ApJS, 54, 259

Fig. 1.— Plot of telluric features removed from all spectra by division of a spectral flat. This figure is the division of a high airmass spectrum by an intermediate airmass spectrum of HR 3454 normalized to unity. The more prominent telluric features are labeled.

Fig. 2.— Averaged blue and red atmospheric extinction curves obtained at CTIO on 5-12 February 1999 (UT).

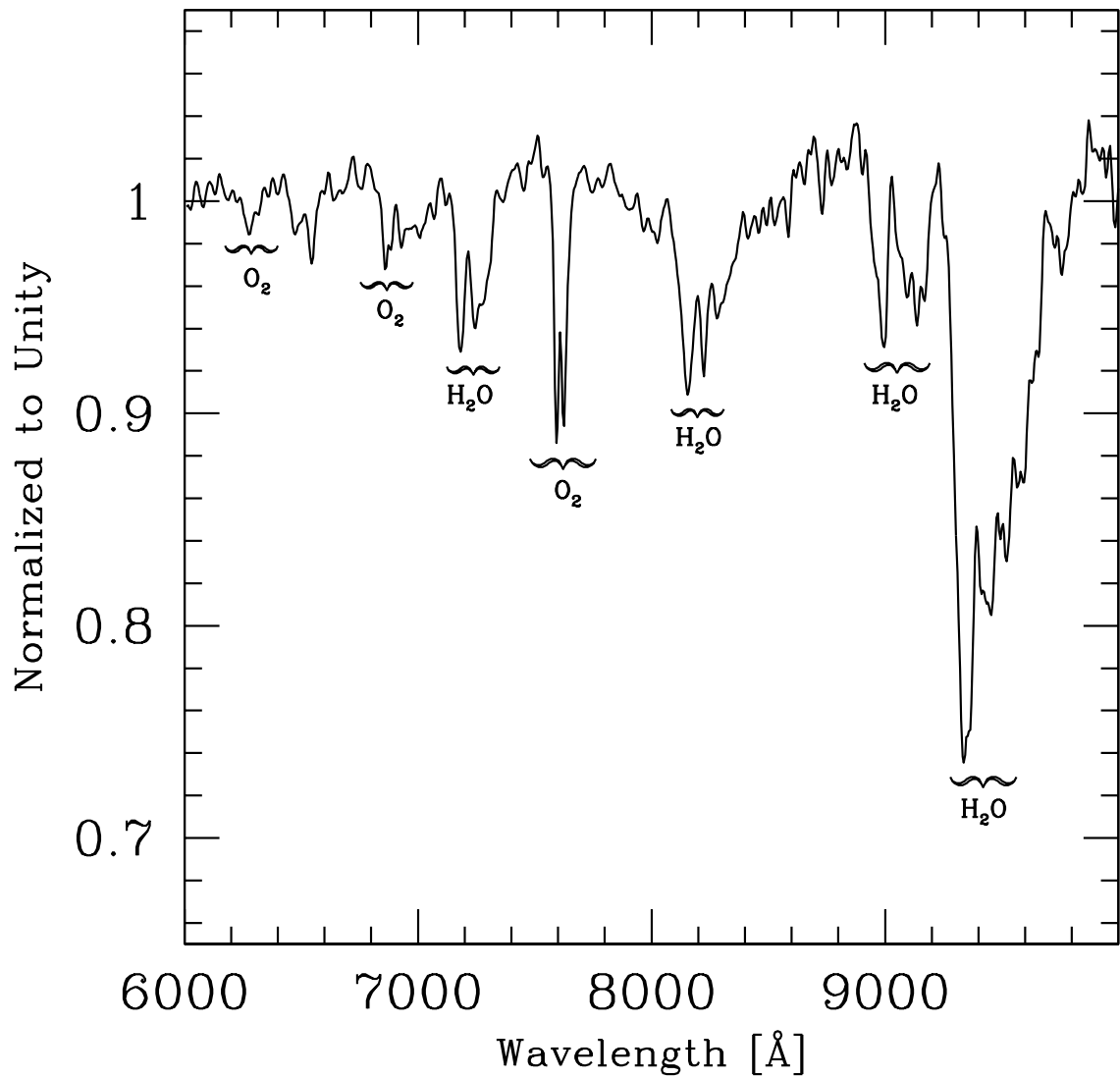
Fig. 3.— Johnson/Kron-Cousins $UBVRI$ standard passbands from Bessell (1990). The Bessell transmission functions have been divided by λ for integrations with photon flux, and multiplied by an atmospheric line opacity spectrum, because they are used with spectra that have had telluric features removed.

Fig. 4.— The difference between observed and synthetic magnitudes derived using the Bessell passbands (see Fig. 3) as a function of color. Significant outliers are variable stars, identified in Table 4.

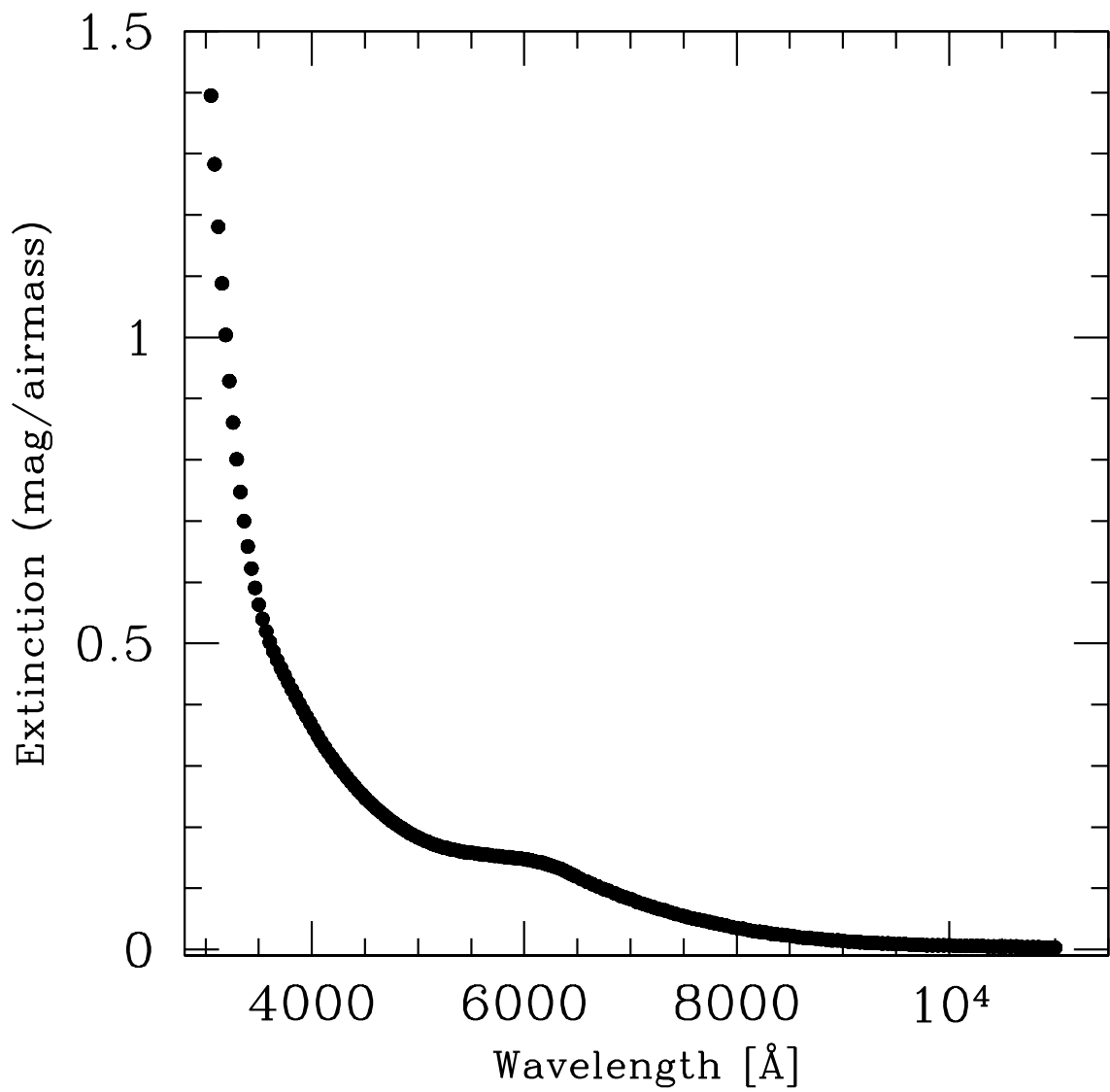
Fig. 5.— Comparison of the Bessell Johnson/Kron-Cousins passbands (dotted lines) to our new modeled passbands (dashed lines) that include the shifts listed in Table 6.

Fig. 6.— V -band observed minus synthetic magnitudes, versus photon counts detected by the LORAL CCD, at the V -band's effective wavelength.

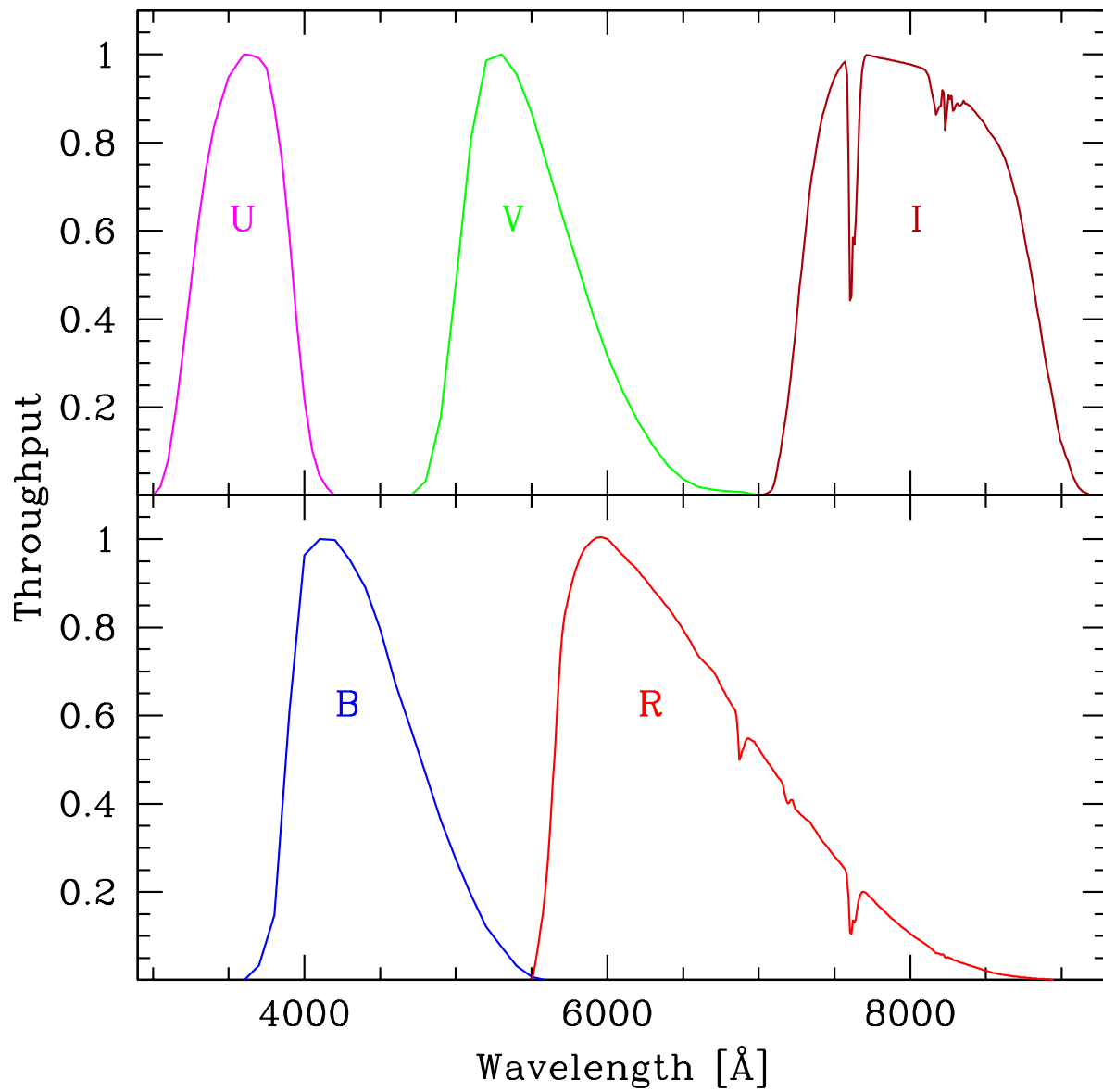
Fig. 7.— Infrared passbands corresponding to Persson et al. (1998) J_S , H , and K_S transmission functions, a NICMOS2 QE, multiple mirror reflections, a Dewar window transmissivity, and an atmospheric line opacity spectrum.



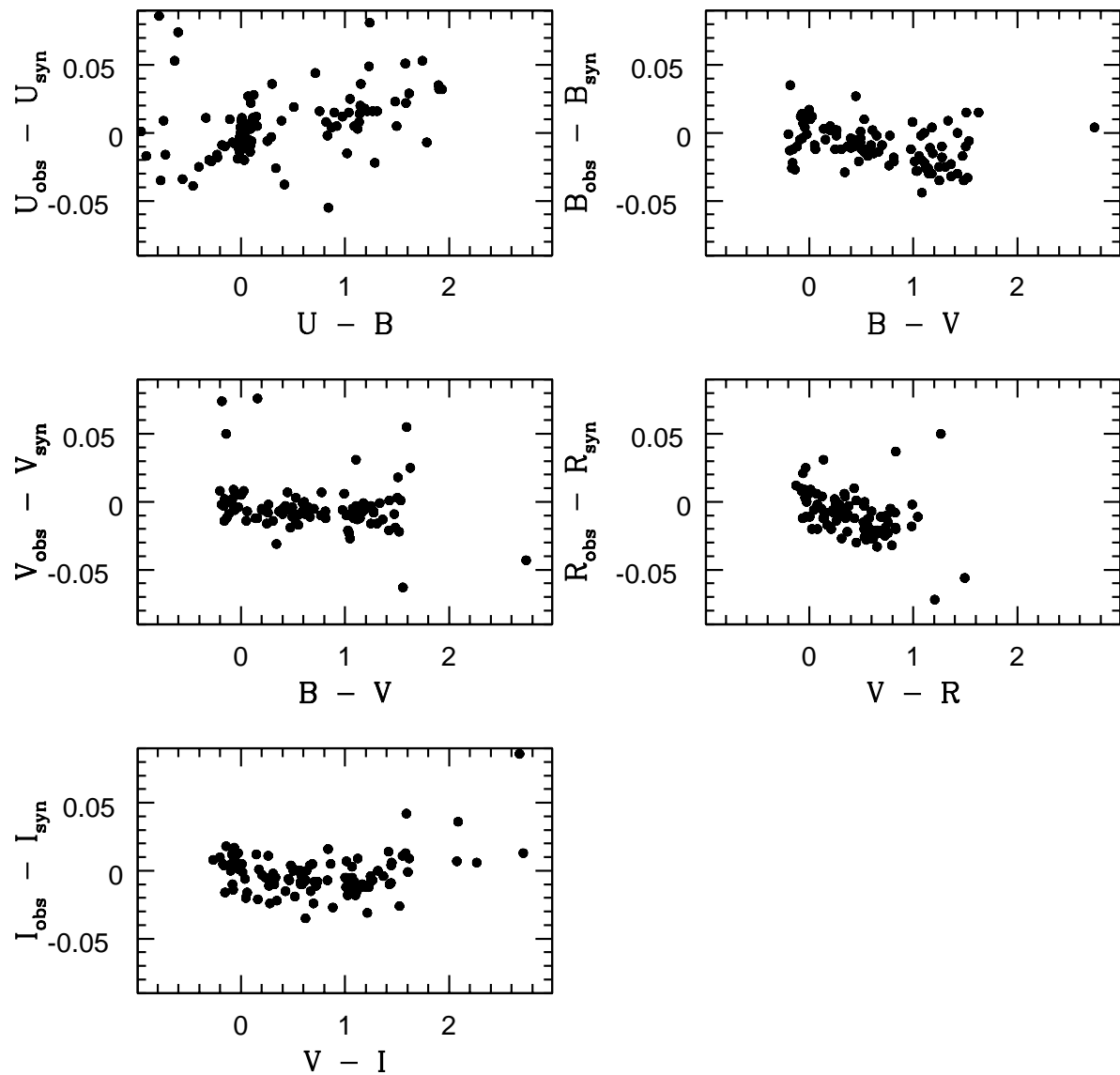
Stritzinger *et al.* Fig. 1



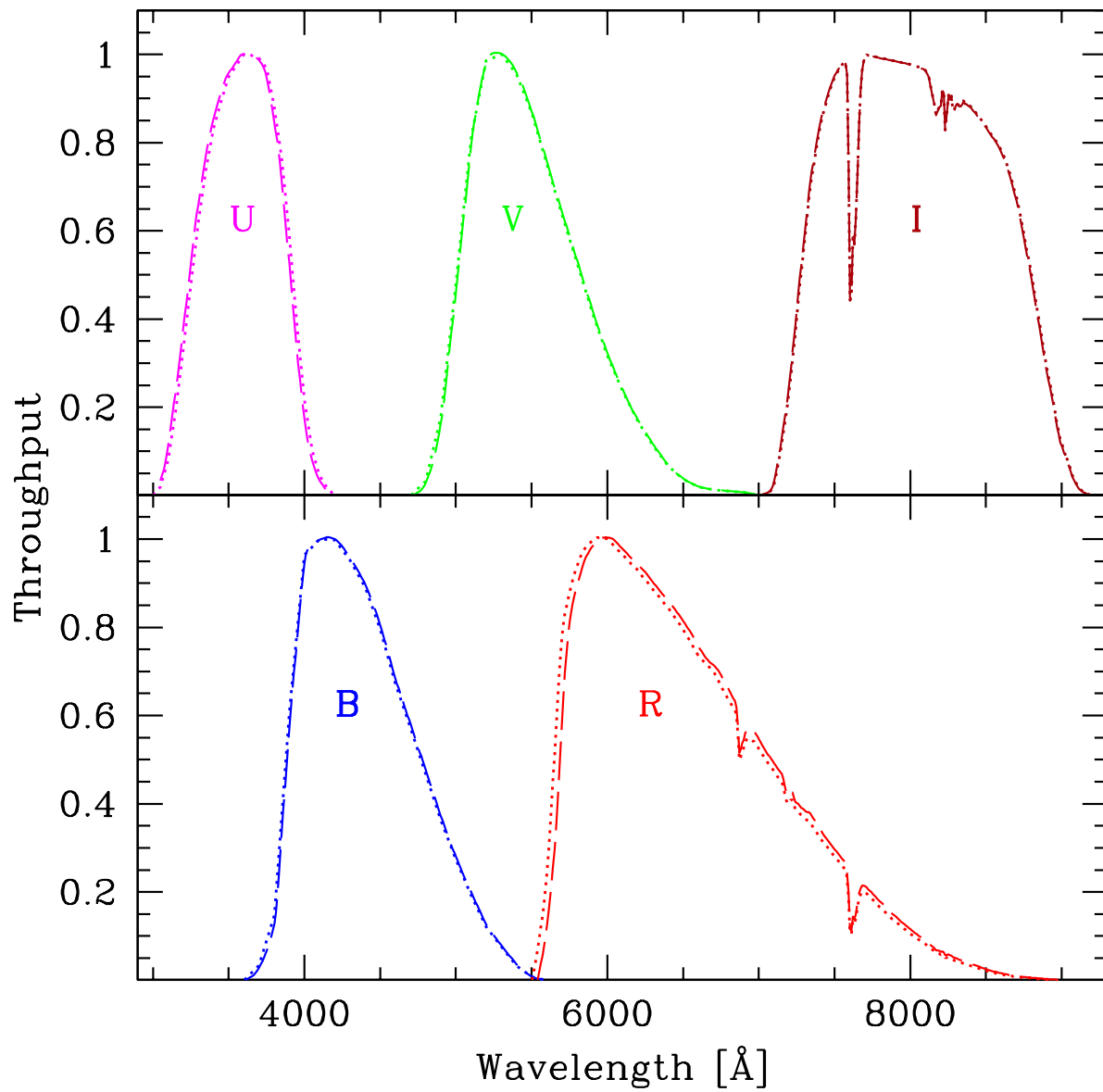
Stritzinger *et al.* Fig. 2



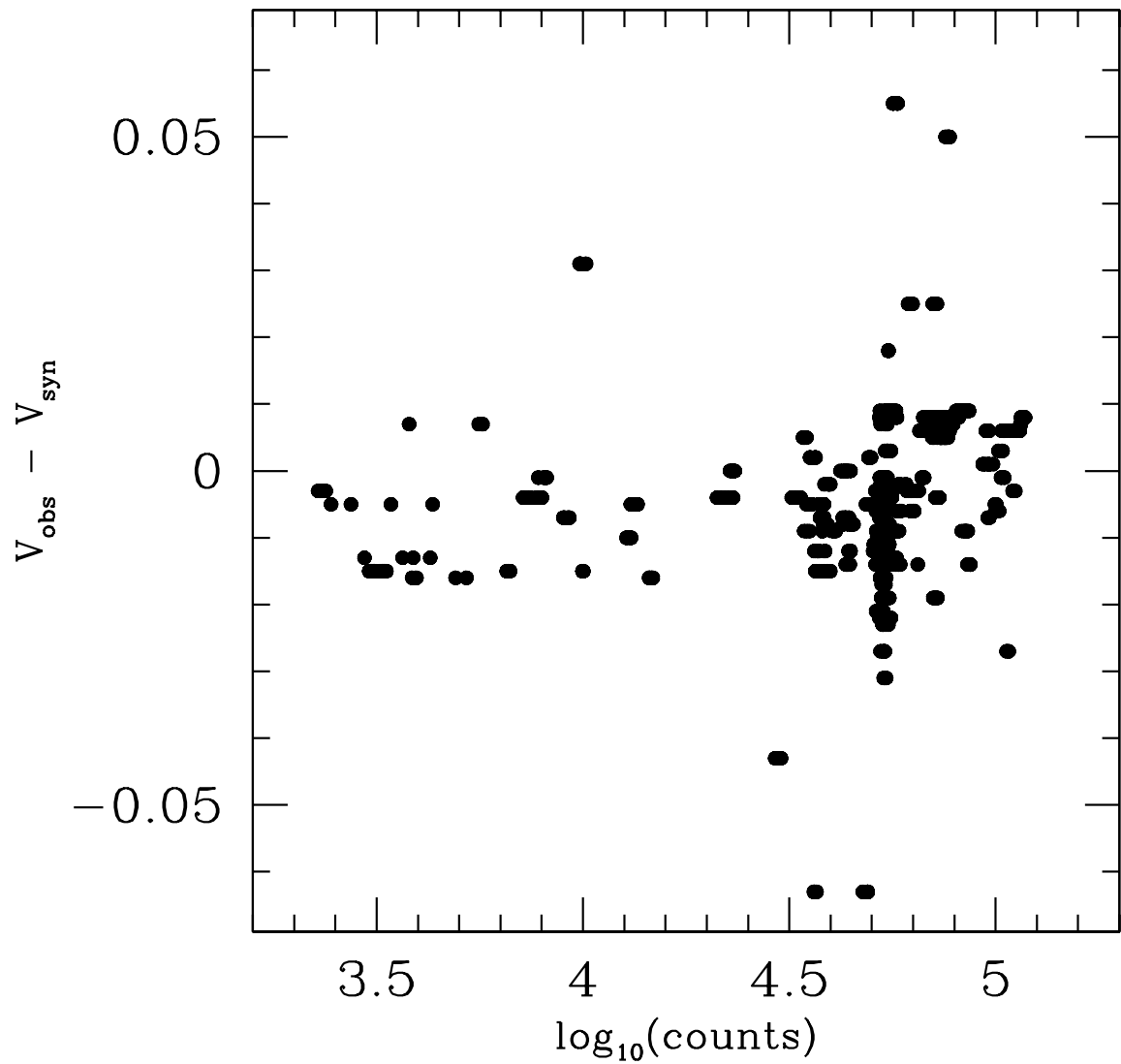
Stritzinger *et al.* Fig. 3



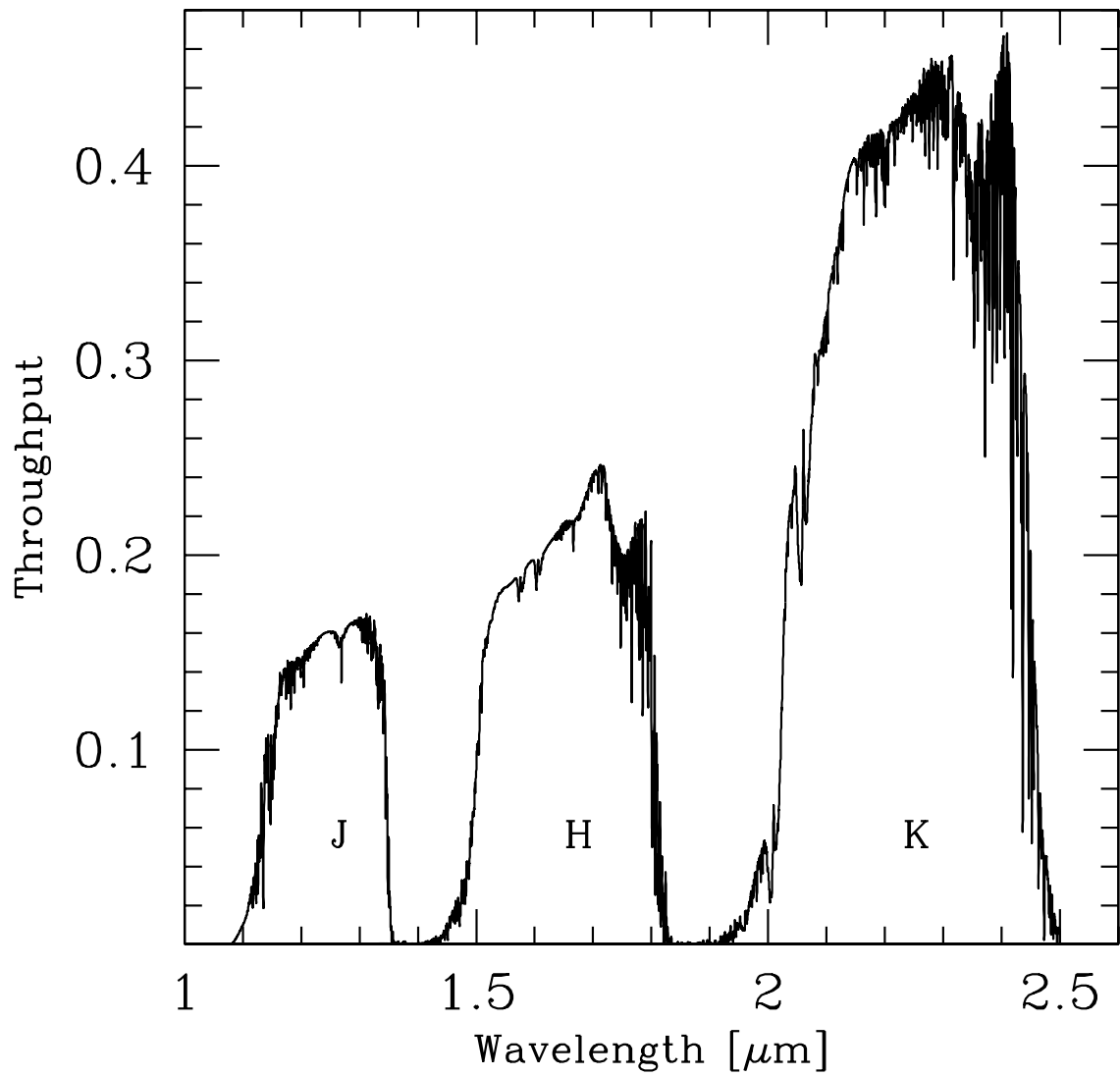
Stritzinger *et al.* Fig. 4



Stritzinger *et al.* Fig. 5



Stritzinger *et al.* Fig. 6



Stritzinger *et al.* Fig. 7

Table 1. Spectrophotometric Secondary Standards

λ [Å]	$\Delta \lambda$	HR 718	HR 1544	HR 3454	HR 4468	HR 4963	HR 5501
3100	45	5.265	5.634	4.080	5.581	5.669	6.737
3150	45	5.256	5.611	4.099	5.576	5.653	6.731
3200	45	5.243	5.589	4.109	5.567	5.637	6.726
3250	45	5.230	5.566	4.125	5.557	5.618	6.717
3300	25	5.218	5.542	4.135	5.552	5.601	6.712
3390	45	5.188	5.519	4.145	5.530	5.563	6.675
3448	45	5.185	5.498	4.168	5.519	5.544	6.667
3509	45	5.175	5.485	4.185	5.517	5.519	6.654
3571	45	5.155	5.466	4.203	5.502	5.499	6.639
3636	45	5.117	5.422	4.197	5.474	5.451	6.608
4036	45	3.930	4.065	3.822	4.337	4.084	5.373
4167	45	3.983	4.110	3.892	4.383	4.123	5.410
4255	45	4.006	4.123	3.916	4.409	4.144	5.427
4464	45	...	4.160	3.983	4.461	4.181	5.476
4566	45	4.091	4.194	4.034	4.502	4.224	5.510
4785	45	4.134	4.222	4.104	4.545	4.247	5.551
5000	45	4.182	4.274	4.175	4.592	4.290	5.587
5264	45	4.235	4.322	4.239	4.653	4.339	5.638
5556	45	4.291	4.363	4.318	4.713	4.376	5.689
5840	45	4.336	4.403	4.388	4.770	4.422	5.738
6058	45	4.393	4.452	4.460	4.822	4.474	5.791
6440	45	4.465	4.516	4.544	4.902	4.543	5.846
6792	45	4.532	4.562	4.623	4.961	4.590	5.889
7102	45	4.593	4.616	4.709	5.019	4.646	5.952
7554	45	4.678	4.693	4.797	5.104	4.718	6.031
7845	45	4.740	4.745	4.861	5.168	4.779	6.065
8092	45	4.766	4.763	4.912	5.194	4.796	6.099
8376	45	4.829	4.825	4.986	5.253	4.847	6.147
8800	10	4.824	4.850	5.039	5.287	4.843	6.177
8920	10	4.827	4.854	5.058	5.298	4.847	6.185
9915	45	4.862	4.867	5.193	5.354	4.888	6.225
9970	45	4.867	4.871	5.202	5.358	4.893	6.231
10150	45	4.891	4.882	5.234	5.378	4.919	6.251
10256	45	4.944	4.898	5.261	5.378	4.926	6.240
10406	45	4.968	4.914	5.296	5.414	4.960	6.271
10500	45	4.986	4.944	5.319	5.443	5.004	6.333
10600	45	5.022	4.965	5.351	5.469	5.041	6.366

Table 1—Continued

λ [Å]	$\Delta \lambda$	HR 718	HR 1544	HR 3454	HR 4468	HR 4963	HR 5501

Note. — All values are in monochromatic magnitudes $m_\nu = -2.5 \log_{10}(f_\nu) - 48.590$.

Table 2. Averaged Extinction Curve for CTIO

λ	Extinction [mag/airmass]
3050.00	1.395
3084.65	1.283
3119.31	1.181
3153.96	1.088
3188.61	1.004
3223.27	0.929
3257.92	0.861
3292.57	0.801
3327.23	0.748
3361.88	0.700
3396.54	0.659
3431.19	0.623
3465.84	0.591
3500.50	0.564
3535.15	0.540
3569.80	0.520
3604.46	0.502
3639.11	0.487
3673.76	0.473
3708.42	0.460
3743.07	0.448
3777.72	0.436
3812.38	0.425
3847.03	0.414
3881.69	0.402
3916.34	0.391
3950.99	0.381
3985.65	0.370
4020.30	0.360
4054.95	0.349
4089.61	0.339
4124.26	0.330
4158.91	0.321
4193.57	0.313
4228.22	0.304
4262.87	0.296
4297.53	0.289

Table 2—Continued

λ	Extinction [mag/airmass]
4332.18	0.281
4366.83	0.274
4401.49	0.267
4436.14	0.260
4470.79	0.254
4505.45	0.247
4540.10	0.241
4574.76	0.236
4609.41	0.230
4644.06	0.225
4678.72	0.220
4713.37	0.215
4748.02	0.210
4782.68	0.206
4817.33	0.202
4851.98	0.198
4886.64	0.194
4921.29	0.190
4955.94	0.187
4990.60	0.184
5025.25	0.181
5059.91	0.178
5094.56	0.176
5129.21	0.173
5163.87	0.171
5198.52	0.169
5233.17	0.167
5267.83	0.166
5302.48	0.164
5337.13	0.163
5371.79	0.162
5406.44	0.160
5441.09	0.159
5475.75	0.158
5510.40	0.158
5545.05	0.157
5579.71	0.156

Table 2—Continued

λ	Extinction [mag/airmass]
5614.36	0.155
5649.02	0.155
5683.67	0.154
5718.32	0.153
5752.98	0.153
5787.63	0.152
5822.28	0.151
5856.94	0.151
5891.59	0.150
5926.24	0.149
5960.90	0.149
5995.55	0.148
6030.20	0.147
6064.86	0.146
6099.51	0.144
6134.17	0.143
6168.82	0.142
6203.47	0.140
6238.13	0.138
6272.78	0.136
6307.43	0.134
6342.09	0.132
6376.74	0.129
6411.39	0.126
6446.05	0.123
6480.70	0.120
6482.85	0.120
6535.38	0.115
6587.91	0.111
6640.44	0.107
6692.96	0.103
6745.49	0.099
6798.02	0.096
6850.55	0.092
6903.07	0.088
6955.60	0.085
7008.13	0.082

Table 2—Continued

λ	Extinction [mag/airmass]
7060.65	0.078
7113.18	0.075
7165.71	0.072
7218.24	0.069
7270.76	0.066
7323.29	0.064
7375.82	0.061
7428.35	0.058
7480.87	0.056
7533.40	0.053
7585.93	0.051
7638.45	0.049
7690.98	0.047
7743.51	0.045
7796.04	0.043
7848.56	0.041
7901.09	0.039
7953.62	0.037
8006.15	0.035
8058.67	0.034
8111.20	0.032
8163.73	0.030
8216.25	0.029
8268.78	0.028
8321.31	0.026
8373.84	0.025
8426.36	0.024
8478.89	0.023
8531.42	0.022
8583.95	0.020
8636.47	0.019
8689.00	0.019
8741.53	0.018
8794.05	0.017
8846.58	0.016
8899.11	0.015
8951.64	0.015

Table 2—Continued

λ	Extinction [mag/airmass]
9004.16	0.014
9056.69	0.013
9109.22	0.013
9161.75	0.012
9214.27	0.011
9266.80	0.011
9319.33	0.011
9371.85	0.010
9424.38	0.010
9476.91	0.009
9529.44	0.009
9581.96	0.009
9634.49	0.008
9687.02	0.008
9739.55	0.008
9792.07	0.007
9844.60	0.007
9897.13	0.007
9949.65	0.007
10002.2	0.007
10054.7	0.006
10107.2	0.006
10159.8	0.006
10212.3	0.006
10264.8	0.006
10317.3	0.006
10369.9	0.005
10422.4	0.005
10474.9	0.005
10527.5	0.005
10580.0	0.005
10632.5	0.005
10685.0	0.004
10737.6	0.004
10790.1	0.004
10842.6	0.004
10895.1	0.003

Table 2—Continued

λ	Extinction [mag/airmass]
10947.7	0.003
11000.2	0.003

Table 3. Zero-points employed in Eq. 3 with standard passbands

Filter	Zero-point
U	–14.244
B	–15.279
V	–14.850
R	–15.053
I	–14.556

Table 4. Synthetic Magnitudes for All Stars[†]

Star	U_{syn}	$U_{\text{obs}}-U_{\text{syn}}$	B_{syn}	$B_{\text{obs}}-B_{\text{syn}}$	V_{syn}	$V_{\text{obs}}-V_{\text{syn}}$	R_{syn}	$R_{\text{obs}}-R_{\text{syn}}$	I_{syn}	$I_{\text{obs}}-I_{\text{syn}}$
bd-0°454	11.849	+0.051	10.321	0	8.894	+0.001	8.152	-0.015	7.446	+0.004
bd+1°2447	12.318	+0.081	11.146	+0.015	9.634	+0.018	8.619	-0.011	7.380	+0.006
bd+5°1668 ^c	12.597	+0.016	11.460	-0.060	9.906	-0.063	8.709	-0.072	7.116	+0.013
bd+5°2468	8.706	-0.034	9.242	-0.010	9.357	-0.009	9.383	+0.003	9.435	+0.005
bd+5°2529	12.001	+0.018	10.866	-0.035	9.584	-0.003	8.805	-0.005	8.125	+0.006
cd-32°9927	10.112	-0.005
eg21	11.526	+0.004
g162-66	11.861	-0.010	12.873	-0.026	13.015	-0.003	13.126	+0.012	13.270	+0.008
hd118246 ^a	7.259	+0.053	7.895	+0.053	8.039	+0.050	8.098	+0.025	8.180	-0.010
hd12021	8.413	-0.025	8.780	+0.012	8.872	+0.002	8.907	+0.009	8.972	0
hd11983	6.627	+0.011
hd121968	9.177	-0.017	10.081	-0.013	10.256	-0.002	10.319	+0.008	10.421	+0.005
hd129975	11.741	+0.035	9.887	-0.010	8.370	+0.003	7.563	-0.019	6.769	-0.001
hd16581	7.853	-0.020	8.131	+0.007	8.201	-0.006	8.220	0	8.254	+0.004
hd21197	10.143	+0.014	9.046	-0.030	7.869	-0.003	7.191	-0.011	6.624	-0.004
hd36395	10.616	+0.049	9.451	-0.017	7.969	-0.009	6.993	-0.018	5.877	+0.007
hd47761 ^b	8.207	+0.074	8.798	+0.085	8.648	+0.076	8.555	+0.031	8.469	-0.024
hd50167	11.087	+0.053	9.402	-0.006	7.860	+0.001	7.043	-0.008	6.265	+0.013
hd52533	6.655	+0.001	7.619	-0.005	7.702	0	7.706	+0.007	7.734	+0.006
hd57884 ^b	9.028	+0.107	7.821	+0.050	6.726	+0.122
hd60826 ^b	9.026	-0.043	7.544	-0.056	6.220	+0.086
hd65079 ^c	6.778	+0.086	7.615	+0.035	7.758	+0.074	7.763	+0.124	7.782	+0.180
hd72055	7.555	-0.039	8.003	-0.027	8.125	-0.012	8.142	+0.002	8.187	+0.012
hd76082	10.612	+0.005	9.553	-0.026	8.422	-0.013	7.851	-0.027	7.326	-0.018
hd79097 ^a	11.130	+0.032	9.214	+0.015	7.576	+0.025	6.613	-0.002	5.478	+0.036
hd84971	7.742	-0.035	8.499	-0.022	8.650	-0.014	8.711	-0.012	8.804	-0.016
hd97503	10.998	+0.003	9.910	-0.030	8.703	-0.001	7.993	-0.011	7.385	0
hr0718	4.106	+0.010	4.209	+0.014	4.272	+0.007	4.294	+0.008	4.331	+0.011

Table 4—Continued

Star	U_{syn}	$U_{\text{obs}}-U_{\text{syn}}$	B_{syn}	$B_{\text{obs}}-B_{\text{syn}}$	V_{syn}	$V_{\text{obs}}-V_{\text{syn}}$	R_{syn}	$R_{\text{obs}}-R_{\text{syn}}$	I_{syn}	$I_{\text{obs}}-I_{\text{syn}}$
hr1544	4.372	-0.008	4.355	+0.010	4.349	+0.006	4.332	+0.009	4.322	-0.006
hr3454	3.343	+0.009	4.096	-0.001	4.287	+0.008	4.368	+0.010	4.485	+0.010
hr4468	4.459	-0.009	4.616	+0.014	4.691	+0.009	4.718	+0.005	4.746	+0.017
hr4963	4.379	-0.014	4.358	+0.017	4.370	+0.005	4.364	+0.008	4.360	+0.005
hr5501	5.585	-0.007	5.659	-0.001	5.685	-0.004	5.688	-0.011	5.694	+0.013
ltt1788	13.349	-0.021	13.618	-0.007
ltt2415	12.388	-0.016	12.604	-0.004
ltt3218	11.646	-0.003
ltt4364	11.189	-0.002
sa94-305	11.876	+0.022	10.342	-0.030	8.910	-0.021	8.155	-0.023	7.455	-0.009
sa94-308	9.229	+0.004	9.241	-0.004	8.754	-0.011	8.459	-0.006	8.177	-0.010
sa94-342	10.706	+0.044	10.026	+0.008	9.035	+0.006	8.517	-0.003	8.019	+0.007
sa95-52	10.145	+0.027	10.093	+0.010	9.571	+0.003	9.273	-0.006	8.971	-0.008
sa95-96	10.234	-0.005	10.154	+0.003	10.022	-0.012	9.933	-0.002	9.835	+0.001
sa95-132	12.776	+0.036	12.485	+0.027	12.057	+0.007	11.805	0	11.519	0
sa95-206	9.259	-0.005	9.251	-0.012	8.748	-0.011	8.449	-0.002	8.162	0
sa96-36	10.946	+0.010	10.836	+0.002	10.598	-0.007	10.469	-0.012	10.331	-0.010
sa96-180 ^c	10.875	-0.055	10.027	-0.048	8.957	-0.027	8.410	-0.028	7.892	-0.013
sa96-235	13.097	+0.015	12.216	-0.002	11.145	-0.005	10.594	-0.013	10.069	+0.003
sa96-393	10.283	+0.007	10.261	-0.013	9.659	-0.007	9.303	+0.004	8.960	+0.005
sa96-406	9.656	+0.012	9.518	+0.002	9.306	-0.006	9.189	-0.005	9.068	-0.005
sa96-737	14.191	+0.019	13.041	+0.009	11.717	-0.001	11.002	-0.019	10.298	-0.010
sa97-249	12.487	-0.003	12.383	+0.003	11.737	-0.002	11.373	-0.004	11.021	-0.005
sa97-346	9.957	+0.011	9.863	-0.009	9.261	-0.001	8.916	+0.006	8.594	+0.004
sa97-351	10.057	+0.022	9.978	+0.005	9.786	-0.005	9.653	+0.004	9.506	+0.011
sa98-193	12.326	+0.036	11.206	+0.004	10.033	-0.003	9.442	-0.027	8.889	-0.012
sa98-320	11.451	+0.008	10.349	-0.026	9.192	-0.012	8.605	-0.021	8.079	-0.015
sa98-653	9.523	-0.001

Table 4—Continued

Star	U_{syn}	$U_{\text{obs}}-U_{\text{syn}}$	B_{syn}	$B_{\text{obs}}-B_{\text{syn}}$	V_{syn}	$V_{\text{obs}}-V_{\text{syn}}$	R_{syn}	$R_{\text{obs}}-R_{\text{syn}}$	I_{syn}	$I_{\text{obs}}-I_{\text{syn}}$
sa98-667	8.059	+0.011	8.394	+0.012	8.370	+0.008	8.301	+0.006	8.217	+0.012
sa98-978	11.284	-0.009	11.179	+0.002	10.572	0	10.235	-0.012	9.916	-0.015
sa99-6	3.612	-0.022	12.328	-0.025	11.070	-0.016	10.435	-0.033	9.837	-0.012
sa99-185	10.388	+0.012	9.445	-0.020	8.354	-0.010	7.799	-0.018	7.278	-0.005
sa99-296	10.890	+0.016	9.656	-0.015	8.460	-0.006	7.861	-0.007	7.322	+0.009
sa99-358	10.871	+0.019	10.383	-0.002	9.598	+0.007	9.163	+0.010	8.751	+0.016
sa99-408	10.257	0	10.223	-0.009	9.812	-0.005	9.553	+0.001	9.306	+0.002
sa99-418	9.289	-0.010	9.429	+0.004	9.469	+0.005	9.471	+0.006	9.489	+0.001
sa99-438	8.534	-0.016	9.255	-0.012	9.396	+0.002	9.436	+0.021	9.521	+0.018
sa99-447	9.143	-0.018	9.354	-0.004	9.422	-0.005	9.460	-0.011	9.505	-0.014
sa100-95	10.111	+0.009	9.750	-0.021	8.927	-0.012	8.492	-0.030	8.058	-0.027
sa100-162	11.918	+0.005	10.444	-0.018	9.158	-0.008	8.522	-0.021	7.959	-0.012
sa100-241	10.403	-0.006	10.301	-0.005	10.151	-0.012	10.081	-0.020	9.997	-0.021
sa100-280	12.291	0	12.292	+0.001	11.803	-0.004	11.510	-0.006	11.221	-0.010
sa100-606	8.790	+0.028	8.702	-0.009	8.655	-0.014	8.635	-0.020	8.613	-0.020
sa101-24	10.127	+0.015	9.127	-0.022	8.000	-0.003	7.434	-0.012	6.914	-0.008
sa101-281	12.844	-0.038	12.405	-0.018	11.582	-0.007	11.122	+0.001	10.706	+0.005
sa101-282	10.430	+0.011	10.436	-0.005	10.005	-0.003	9.756	-0.014	9.501	-0.019
sa101-311	8.492	+0.009	8.496	+0.002	8.235	-0.002	8.082	-0.008	7.921	-0.010
sa101-324	12.031	+0.020	10.914	-0.011	9.750	-0.008	9.174	-0.023	8.643	-0.011
sa101-333	11.114	-0.007	9.355	-0.035	7.854	-0.019	7.072	-0.032	6.337	-0.026
sa101-363	10.255	+0.009	10.137	-0.002	9.882	-0.008	9.740	-0.012	9.587	-0.010
sa101-389	10.397	-0.009	10.399	-0.010	9.967	-0.005	9.707	-0.001	9.459	0
sa102-58	9.470	-0.009	9.452	-0.012	9.387	-0.007	9.342	-0.006	9.336	-0.016
sa102-276	10.389	-0.011	10.409	-0.007	9.915	-0.005	9.625	-0.006	9.343	-0.008
sa102-381	8.315	+0.005	8.237	-0.012	7.930	-0.014	7.760	-0.017	7.592	-0.022
sa102-466	11.218	+0.005	10.319	-0.017	9.255	-0.009	8.701	-0.018	8.184	-0.007
sa102-472	10.579	+0.008	9.789	-0.021	8.764	-0.010	8.246	-0.020	7.755	-0.012

Table 4—Continued

Star	U_{syn}	$U_{\text{obs}}-U_{\text{syn}}$	B_{syn}	$B_{\text{obs}}-B_{\text{syn}}$	V_{syn}	$V_{\text{obs}}-V_{\text{syn}}$	R_{syn}	$R_{\text{obs}}-R_{\text{syn}}$	I_{syn}	$I_{\text{obs}}-I_{\text{syn}}$
sa102-620	12.187	-0.015	11.196	-0.044	10.081	-0.012	9.450	-0.023	8.912	-0.010
sa102-625	9.477	0	9.454	-0.012	8.907	-0.017	8.605	-0.027	8.304	-0.035
sa102-1081	10.828	-0.006	10.581	-0.014	9.914	-0.011	9.559	-0.022	9.229	-0.024
sa103-302	10.181	-0.008	10.239	-0.010	9.868	-0.007	9.639	-0.006	9.403	-0.007
sa103-462	10.778	-0.014	10.692	-0.017	10.120	-0.009	9.794	-0.007	9.481	0
sa103-483	8.870	+0.003	8.785	-0.005	8.359	-0.006	8.106	+0.002	7.869	+0.004
sa104-306 ^b	12.447	+0.181	10.876	+0.086	9.315	+0.055	8.501	+0.037	7.737	+0.042
sa104-337	12.337	-0.026	11.999	-0.024	11.217	-0.010	10.785	-0.012	10.382	-0.007
sa104-461	10.170	-0.019	10.202	-0.021	9.724	-0.019	9.427	-0.011	9.128	-0.003
sa104-598	13.610	+0.025	12.585	0	11.448	+0.031	10.832	-0.023	10.295	-0.031
sa105-28	10.250	+0.004	9.412	-0.028	8.368	-0.023	7.833	-0.021	7.332	-0.005
sa105-66	9.155	-0.020	9.131	-0.029	8.791	-0.031	8.569	-0.020	8.346	-0.015
sa105-205	11.748	+0.029	10.193	-0.032	8.811	-0.013	8.064	-0.010	7.365	+0.014
sa105-214	7.583	-0.003	7.604	-0.014	7.077	-0.015	6.759	-0.010	6.445	-0.007
sa105-405	11.703	+0.032	9.863	-0.033	8.331	-0.022	7.497	-0.020	6.683	+0.009
sa105-448	9.457	+0.005	9.437	-0.012	9.192	-0.016	9.035	-0.008	8.869	-0.004
sa105-663	11.143	+0.016	10.415	-0.012	9.432	-0.006	8.919	-0.015	8.428	-0.005
sa106-575	12.109	+0.023	10.674	-0.025	9.357	-0.016	8.691	-0.022	8.083	-0.007
sa106-700	12.678	+0.051	11.170	-0.023	9.798	-0.013	9.082	-0.025	8.419	-0.004
sa106-834	10.084	-0.003	9.798	-0.009	9.093	-0.005	8.712	-0.003	8.360	-0.008
sa106-1250	9.986	-0.002	9.180	-0.028	8.144	-0.021	7.617	-0.026	7.115	-0.018
sa107-35	10.347	+0.016	9.064	-0.010	7.786	-0.007	7.137	-0.021	6.537	-0.007
sa107-544	9.589	+0.005	9.449	-0.011	9.046	-0.009	8.812	-0.008	8.586	-0.006
sa107-684	9.136	-0.012	9.067	-0.015	8.442	-0.009	8.085	-0.008	7.733	-0.008

[†]Observed magnitudes taken from Landolt (1983), Landolt (1992a), Landolt (1992b), Hamuy et al. (1992) & Landolt (1999).

^aLandolt (1983) lists as possible variable.

^bLandolt (1983) lists as variable.

^cPossible variable star.

Table 5. Mean differences and standard deviations between observed and synthetic magnitudes

Filter	Mean Difference	s. d.
<i>U</i>	+0.007	0.023
<i>B</i>	−0.010	0.011
<i>V</i>	−0.006	0.006
<i>R</i>	−0.008	0.010
<i>I</i>	−0.003	0.007

Note. — Mean values were determined utilizing an outlier resistance algorithm. Standard deviations were determined using a robust sigma algorithm.

Table 6. Wavelength shifts applied to Bessell passbands

Passband	Shift [Å]	
<i>U</i>	16	blue
<i>B</i>	8.5	red
<i>V</i>	6	red
<i>R</i>	38	red
<i>I</i>	5	blue

Table 7. Normalized UBV Standard Passbands

λ	U	λ	B	λ	V
3000	0.000	3600	0.000	4700	0.000
3050	0.034	3700	0.028	4800	0.027
3100	0.113	3800	0.126	4900	0.160
3150	0.236	3900	0.569	5000	0.462
3200	0.376	4000	0.945	5100	0.790
3250	0.525	4100	0.998	5200	0.979
3300	0.662	4200	1.000	5300	1.000
3350	0.770	4300	0.958	5400	0.960
3400	0.855	4400	0.898	5500	0.873
3450	0.913	4500	0.806	5600	0.759
3500	0.958	4600	0.685	5700	0.645
3550	0.983	4700	0.581	5800	0.533
3600	1.000	4800	0.478	5900	0.422
3650	0.997	4900	0.373	6000	0.324
3700	0.987	5000	0.280	6100	0.241
3750	0.947	5200	0.127	6200	0.173
3800	0.851	5300	0.079	6300	0.118
3850	0.713	5400	0.037	6400	0.070
3900	0.526	5500	0.009	6500	0.039
3950	0.334	5600	0.000	6600	0.021
4000	0.175	6700	0.013
4050	0.080	6800	0.010
4100	0.035	6900	0.007
4150	0.010	7000	0.000
4200	0.000

Table 8. Normalized R & I Standard Passband

λ	R	λ	I
5501.5	-0.052	7001.9	0.000
5511.5	-0.040	7011.9	0.001
5521.5	-0.026	7021.9	0.002
5531.5	-0.012	7031.9	0.003
5541.5	0.003	7041.9	0.004
5551.5	0.019	7051.9	0.005
5561.5	0.037	7061.9	0.007
5571.5	0.056	7071.9	0.010
5581.5	0.077	7081.9	0.014
5591.5	0.100	7091.9	0.021
5601.5	0.125	7101.9	0.034
5611.5	0.152	7111.9	0.048
5621.5	0.182	7121.9	0.066
5631.5	0.216	7131.9	0.087
5641.5	0.254	7141.9	0.109
5651.5	0.298	7151.9	0.132
5661.5	0.348	7161.9	0.155
5671.5	0.404	7171.9	0.176
5681.5	0.463	7181.9	0.197
5691.5	0.524	7191.9	0.222
5701.5	0.585	7201.9	0.252
5711.5	0.644	7211.9	0.290
5721.5	0.699	7221.9	0.326
5731.5	0.747	7231.9	0.355
5741.5	0.785	7241.9	0.385
5751.5	0.813	7251.9	0.423
5761.5	0.835	7261.9	0.460
5771.5	0.853	7271.9	0.494
5781.5	0.869	7281.9	0.528
5791.5	0.883	7291.9	0.561
5801.5	0.896	7301.9	0.591
5811.5	0.909	7311.9	0.621
5821.5	0.921	7321.9	0.653
5831.5	0.932	7331.9	0.687
5841.5	0.943	7341.9	0.713
5851.5	0.953	7351.9	0.737

Table 8—Continued

λ	R	λ	I
5861.5	0.961	7361.9	0.759
5871.5	0.968	7371.9	0.781
5881.5	0.974	7381.9	0.801
5891.5	0.979	7391.9	0.820
5901.5	0.983	7401.9	0.837
5911.5	0.987	7411.9	0.854
5921.5	0.991	7421.9	0.868
5931.5	0.995	7431.9	0.881
5941.5	0.998	7441.9	0.894
5951.5	1.000	7451.9	0.905
5961.5	1.002	7461.9	0.916
5971.5	1.003	7471.9	0.926
5981.5	1.004	7481.9	0.935
5991.5	1.004	7491.9	0.944
6001.5	1.004	7501.9	0.952
6011.5	1.003	7511.9	0.959
6021.5	1.003	7521.9	0.965
6031.5	1.001	7531.9	0.970
6041.5	1.000	7541.9	0.975
6051.5	0.996	7551.9	0.979
6061.5	0.992	7561.9	0.982
6071.5	0.989	7571.9	0.986
6081.5	0.985	7581.9	0.954
6091.5	0.981	7591.9	0.751
6101.5	0.978	7601.9	0.443
6111.5	0.975	7611.9	0.452
6121.5	0.970	7621.9	0.585
6131.5	0.967	7631.9	0.570
6141.5	0.963	7641.9	0.626
6151.5	0.960	7651.9	0.743
6161.5	0.956	7661.9	0.847
6171.5	0.953	7671.9	0.919
6181.5	0.949	7681.9	0.963
6191.5	0.946	7691.9	0.983
6201.5	0.942	7701.9	0.995
6211.5	0.939	7711.9	0.999
6221.5	0.936	7721.9	0.998

Table 8—Continued

λ	R	λ	I
6231.5	0.932	7731.9	0.997
6241.5	0.928	7741.9	0.996
6251.5	0.924	7751.9	0.996
6261.5	0.920	7761.9	0.995
6271.5	0.915	7771.9	0.994
6281.5	0.911	7781.9	0.993
6291.5	0.907	7791.9	0.992
6301.5	0.902	7801.9	0.992
6311.5	0.898	7811.9	0.991
6321.5	0.894	7821.9	0.990
6331.5	0.889	7831.9	0.990
6341.5	0.885	7841.9	0.989
6351.5	0.881	7851.9	0.988
6361.5	0.877	7861.9	0.988
6371.5	0.873	7871.9	0.987
6381.5	0.868	7881.9	0.986
6391.5	0.864	7891.9	0.985
6401.5	0.860	7901.9	0.985
6411.5	0.856	7911.9	0.984
6421.5	0.852	7921.9	0.983
6431.5	0.848	7931.9	0.982
6441.5	0.843	7941.9	0.982
6451.5	0.839	7951.9	0.981
6461.5	0.834	7961.9	0.980
6471.5	0.829	7971.9	0.979
6481.5	0.824	7981.9	0.978
6491.5	0.819	7991.9	0.978
6501.5	0.814	8001.9	0.977
6511.5	0.809	8011.9	0.976
6521.5	0.804	8021.9	0.974
6531.5	0.798	8031.9	0.973
6541.5	0.793	8041.9	0.972
6551.5	0.788	8051.9	0.971
6561.5	0.782	8061.9	0.970
6571.5	0.776	8071.9	0.969
6581.5	0.770	8081.9	0.967
6591.5	0.764	8091.9	0.966

Table 8—Continued

λ	R	λ	I
6601.5	0.758	8101.9	0.963
6611.5	0.752	8111.9	0.955
6621.5	0.746	8121.9	0.949
6631.5	0.740	8131.9	0.932
6641.5	0.735	8141.9	0.915
6651.5	0.731	8151.9	0.900
6661.5	0.727	8161.9	0.884
6671.5	0.723	8171.9	0.862
6681.5	0.720	8181.9	0.873
6691.5	0.717	8191.9	0.881
6701.5	0.714	8201.9	0.883
6711.5	0.711	8211.9	0.919
6721.5	0.707	8221.9	0.912
6731.5	0.703	8231.9	0.827
6741.5	0.698	8241.9	0.863
6751.5	0.692	8251.9	0.907
6761.5	0.686	8261.9	0.897
6771.5	0.679	8271.9	0.905
6781.5	0.673	8281.9	0.872
6791.5	0.666	8291.9	0.875
6801.5	0.659	8301.9	0.884
6811.5	0.653	8311.9	0.888
6821.5	0.646	8321.9	0.883
6831.5	0.640	8331.9	0.882
6841.5	0.633	8341.9	0.886
6851.5	0.618	8351.9	0.893
6861.5	0.577	8361.9	0.887
6871.5	0.515	8371.9	0.887
6881.5	0.524	8381.9	0.884
6891.5	0.538	8391.9	0.882
6901.5	0.545	8401.9	0.879
6911.5	0.559	8411.9	0.873
6921.5	0.568	8421.9	0.870
6931.5	0.570	8431.9	0.867
6941.5	0.569	8441.9	0.861
6951.5	0.567	8451.9	0.858
6961.5	0.566	8461.9	0.854

Table 8—Continued

λ	R	λ	I
6971.5	0.564	8471.9	0.849
6981.5	0.558	8481.9	0.844
6991.5	0.552	8491.9	0.838
7001.5	0.546	8501.9	0.833
7011.5	0.540	8511.9	0.828
7021.5	0.534	8521.9	0.823
7031.5	0.528	8531.9	0.818
7041.5	0.522	8541.9	0.813
7051.5	0.517	8551.9	0.808
7061.5	0.512	8561.9	0.803
7071.5	0.507	8571.9	0.798
7081.5	0.502	8581.9	0.792
7091.5	0.497	8591.9	0.786
7101.5	0.492	8601.9	0.778
7111.5	0.487	8611.9	0.770
7121.5	0.482	8621.9	0.761
7131.5	0.477	8631.9	0.751
7141.5	0.472	8641.9	0.741
7151.5	0.468	8651.9	0.731
7161.5	0.457	8661.9	0.719
7171.5	0.441	8671.9	0.708
7181.5	0.426	8681.9	0.695
7191.5	0.418	8691.9	0.682
7201.5	0.419	8701.9	0.667
7211.5	0.426	8711.9	0.652
7221.5	0.426	8721.9	0.635
7231.5	0.414	8731.9	0.618
7241.5	0.404	8741.9	0.601
7251.5	0.402	8751.9	0.583
7261.5	0.399	8761.9	0.564
7271.5	0.395	8771.9	0.545
7281.5	0.391	8781.9	0.527
7291.5	0.388	8791.9	0.507
7301.5	0.385	8801.9	0.488
7311.5	0.382	8811.9	0.468
7321.5	0.381	8821.9	0.448
7331.5	0.381	8831.9	0.427

Table 8—Continued

λ	R	λ	I
7341.5	0.377	8841.9	0.405
7351.5	0.372	8851.9	0.384
7361.5	0.367	8861.9	0.361
7371.5	0.361	8871.9	0.340
7381.5	0.356	8881.9	0.320
7391.5	0.350	8891.9	0.300
7401.5	0.345	8901.9	0.281
7411.5	0.339	8911.9	0.263
7421.5	0.334	8921.9	0.246
7431.5	0.328	8931.9	0.227
7441.5	0.323	8941.9	0.210
7451.5	0.319	8951.9	0.192
7461.5	0.314	8961.9	0.171
7471.5	0.310	8971.9	0.152
7481.5	0.305	8981.9	0.139
7491.5	0.301	8991.9	0.120
7501.5	0.296	9001.9	0.110
7511.5	0.292	9011.9	0.099
7521.5	0.288	9021.9	0.089
7531.5	0.284	9031.9	0.079
7541.5	0.279	9041.9	0.073
7551.5	0.275	9051.9	0.063
7561.5	0.271	9061.9	0.053
7571.5	0.267	9071.9	0.042
7581.5	0.254	9081.9	0.033
7591.5	0.199	9091.9	0.027
7601.5	0.116	9101.9	0.021
7611.5	0.112	9111.9	0.016
7621.5	0.144	9121.9	0.013
7631.5	0.139	9131.9	0.010
7641.5	0.148	9141.9	0.008
7651.5	0.173	9151.9	0.006
7661.5	0.194	9161.9	0.004
7671.5	0.208	9171.9	0.003
7681.5	0.214	9181.9	0.002
7691.5	0.215	9191.9	0.001
7701.5	0.214	9201.9	0.000

Table 8—Continued

λ	R	λ	I
7711.5	0.211
7721.5	0.207
7731.5	0.204
7741.5	0.200
7751.5	0.196
7761.5	0.193
7771.5	0.189
7781.5	0.185
7791.5	0.182
7801.5	0.178
7811.5	0.175
7821.5	0.171
7831.5	0.168
7841.5	0.165
7851.5	0.161
7861.5	0.158
7871.5	0.155
7881.5	0.151
7891.5	0.148
7901.5	0.145
7911.5	0.142
7921.5	0.139
7931.5	0.136
7941.5	0.133
7951.5	0.130
7961.5	0.127
7971.5	0.124
7981.5	0.121
7991.5	0.118
8001.5	0.115
8011.5	0.113
8021.5	0.110
8031.5	0.107
8041.5	0.105
8051.5	0.102
8061.5	0.100
8071.5	0.097

Table 8—Continued

λ	R	λ	I
8081.5	0.095
8091.5	0.092
8101.5	0.090
8111.5	0.087
8121.5	0.085
8131.5	0.081
8141.5	0.078
8151.5	0.075
8161.5	0.072
8171.5	0.068
8181.5	0.067
8191.5	0.066
8201.5	0.065
8211.5	0.066
8221.5	0.064
8231.5	0.056
8241.5	0.057
8251.5	0.058
8261.5	0.056
8271.5	0.055
8281.5	0.052
8291.5	0.051
8301.5	0.050
8311.5	0.049
8321.5	0.047
8331.5	0.046
8341.5	0.045
8351.5	0.044
8361.5	0.042
8371.5	0.041
8381.5	0.040
8391.5	0.039
8401.5	0.037
8411.5	0.036
8421.5	0.035
8431.5	0.033
8441.5	0.032

Table 8—Continued

λ	R	λ	I
8451.5	0.031
8461.5	0.030
8471.5	0.029
8481.5	0.027
8491.5	0.026
8501.5	0.025
8511.5	0.024
8521.5	0.023
8531.5	0.022
8541.5	0.021
8551.5	0.020
8561.5	0.019
8571.5	0.018
8581.5	0.017
8591.5	0.016
8601.5	0.016
8611.5	0.015
8621.5	0.014
8631.5	0.013
8641.5	0.013
8651.5	0.012
8661.5	0.012
8671.5	0.011
8681.5	0.011
8691.5	0.010
8701.5	0.010
8711.5	0.009
8721.5	0.009
8731.5	0.008
8741.5	0.008
8751.5	0.007
8761.5	0.007
8771.5	0.007
8781.5	0.006
8791.5	0.006
8801.5	0.006
8811.5	0.005

Table 8—Continued

λ	R	λ	I
8821.5	0.005
8831.5	0.005
8841.5	0.004
8851.5	0.004
8861.5	0.004
8871.5	0.004
8881.5	0.003
8891.5	0.003
8901.5	0.003
8911.5	0.003
8921.5	0.002
8931.5	0.002
8941.5	0.002
8951.5	0.002
8961.5	0.001
8971.5	0.001
8981.5	0.000
8991.5	0.000
9001.5	0.000

Table 9. Filter Shifts

Passband	Shift [Å]	Color Term
<i>U</i>	12	$(U - B)$
<i>B</i>	7.4	$(B - V)$
<i>V</i>	15.2	$(B - V)$
<i>R</i>	12.4	$(V - R)$
<i>I</i>	40.5	$(V - I)$

Note. — All shifts to the red.

Table 10. Spectrophotometry of the Sun, Sirius & Vega

passband	<i>U</i>	<i>B</i>	<i>V</i>	<i>R</i>	<i>I</i>	<i>J</i>	<i>H</i>	<i>K</i>	ref.
Sun									
m_{obs}	-25.947	-26.104	-26.755	-27.118	-27.464	-27.885	-28.219	-28.261	1
m_{syn}	-25.983	-26.099	-26.763	-27.125	-27.455	-27.939	-28.260	-28.307	
$m_{\text{obs}} - m_{\text{syn}}$	+0.021	+0.001	+0.009	+0.003	-0.008	+0.054	+0.041	+0.046	
Sirius									
m_{obs}	-1.480	-1.435	-1.430	-1.419	-1.412	-1.385	-1.382	-1.367	2
m_{syn}	-1.463	-1.435	-1.425	-1.406	-1.373	-1.392	-1.381	-1.377	
$m_{\text{obs}} - m_{\text{syn}}$	-0.042	0	-0.007	-0.029	-0.038	+0.007	-0.001	+0.010	
Vega									
m_{obs}	+0.025	+0.025	+0.030	+0.039	+0.035	-0.001	0	-0.001	3
m_{syn}	+0.058	+0.003	+0.024	+0.037	+0.046	0	0	0	
$m_{\text{obs}} - m_{\text{syn}}$	-0.063	+0.022	+0.004	-0.013	-0.010	-0.001	0	-0.001	

References. — (1) Averaged values from Table A3 of Bessell et al. (1998) referenced from Stebbins & Kron (1957), Colina et al. (1996) & Cayrel de Strobel (1996); (2) Table A2 Bessell et al. (1998) & references within, *UBRI* averaged values, *JHK* Table A1 Cohen et al. (1999); (3) Table A2 Bessell et al. 1998, *B* averaged value, *JHK* Table A2 Cohen et al. (1999).